

# Superconducting Spin-Singlet Qubit in a Triangulene Spin Chain

Chen-How Huang,<sup>1,2</sup> Jon Ortuzar,<sup>3</sup> and M. A. Cazalilla<sup>1,4</sup>

<sup>1</sup>*Donostia International Physics Center (DIPC), 20018 Donostia-San Sebastián, Spain*

<sup>2</sup>*Departamento de Polmeros y Materiales Avanzados: Física, Química y Tecnología, Facultad de Ciencias Químicas,*

*Universidad del País Vasco UPV/EHU, 20018 Donostia-San Sebastián, Spain.*

<sup>3</sup>*CIC nanoGUNE-BRTA, 20018 Donostia-San Sebastián, Spain*

<sup>4</sup>*IKERBASQUE, Basque Foundation for Science, Plaza Euskadi 5 48009 Bilbao, Spain*

(Dated: April 1, 2025)

Chains of triangular nanographene (triangulene), recently identified as realizing the valence-bond solid phase of a spin-1 chain, offer a promising platform for quantum information processing. We propose a superconducting spin-singlet qubit based on these chains grown on a superconducting substrate. Using the numerical renormalization group (NRG), we find a manifold of two lowest-lying, isolated spin-singlet states that undergo an avoided crossing. A qubit utilizing these states is thus protected from random-field noise and quasi-particle poisoning. We also introduce a mesoscopic device architecture, based on a triple quantum dot coupled to a superconducting junction, that quantum simulates the spin chain and enables control and readout of the qubit. An effective two-level description of the device is validated using time-dependent NRG.

**Introduction:** Chains of magnetic atoms and molecules have attracted considerable interest due to their potential to host exotic excitations and phases [1–5]. Their low dimensionality enhances strong electron correlation effects [1], resulting in rich quantum behavior and offering promising platforms for realizing topological phases of matter [4–7]. Indeed, fabricating magnetic chains on superconductors may allow the engineering of decoherence-free quantum memories [6] in topological superconductors hosting Majorana bound states [8, 9].

Building on recent advances, the on-surface synthesis technique [10, 11] allows for precise engineering of carbon-based molecules, enabling the manipulation of their magnetic properties. The spin state of several types of nanographene structures can be controlled in this way [12–14]. Recently, the authors of Ref. [15] have demonstrated that a spin chain can be grown from triangulenes (i.e., triangular forms of nanographene). The triangulene spin chains (TSCs) were shown to realize the valence-bond solid (VBS) phase of a spin-1 chain [2–5], with open TSCs hosting topological spin- $\frac{1}{2}$  edge states [15, 16]. Since the TSCs are grown on a metallic [Au(111)] surface, the spin- $\frac{1}{2}$  edge states undergo Kondo screening [17] observed as Kondo resonances near the triangulene terminal units [15]. In addition, recent experiments indicate that thin, pristine Ag(111) and Au(111) films can be proximitized by bulk superconductors [18–22], which hints at the possibility of growing TSCs via on-surface synthesis on superconductors.

In parallel with these developments, significant progress has been made in spin qubits (SQs) since the seminal work by Loss and DiVincenzo [23]. Various SQ platforms have been explored and continuous improvements in quantum coherence and addressability have been demonstrated [24–29]. Despite these advances, decoherence is a major challenge whose main cause is the

Overhauser-field noise arising from spin-orbit interaction [30, 31] and hyperfine coupling with the nuclei in the quantum dot [32, 33]. One possible way out of this conundrum is to design qubits based on spin-singlet states [34] which, to leading order, are immune to the Overhauser-field noise.

In this manuscript, we propose a spin-singlet qubit based on a TSC grown on a superconductor; see Fig. 1(b). Unlike a previous proposal based on ‘Shiba molecules’ of magnetic adatoms [35], we do not necessarily rely on the Ruderman-Kittel-Kasuya-Yosida (RKKY) interaction, whose sign and strength are difficult to control

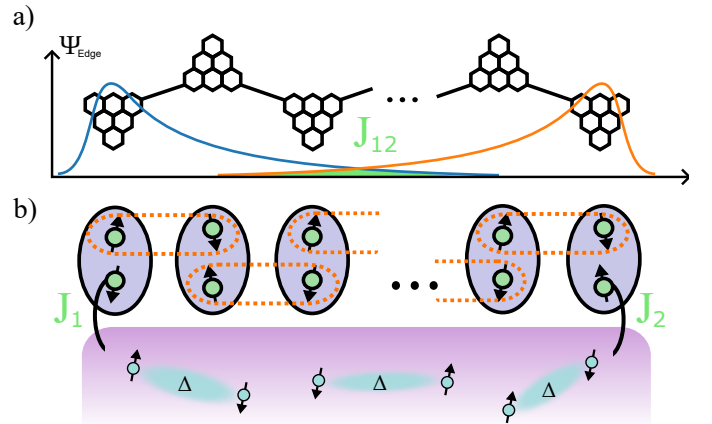


FIG. 1. (a) Sketch of an open triangulene spin chain (TSC, see e.g. [15]). For sufficiently long chains, it hosts two spin- $\frac{1}{2}$  states that are exponentially localized near the edges. (b) Illustration of the TSC on a superconductor. The edge states couple to the superconductor via Kondo exchange remains. Since the latter is weaker than the anti-ferromagnetic exchange between the inner spin-1 triangulenes, the central region remains decoupled in a valence bond solid (VBS) phase.

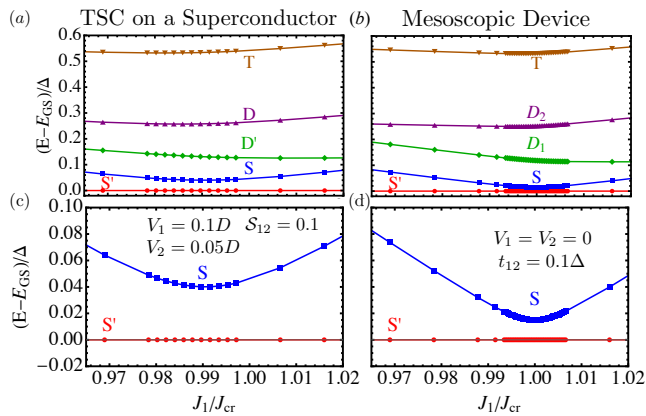


FIG. 2. Low-lying spectrum for  $J_{12} = \Delta = 0.025D$  and  $J_2 = 20\Delta$ : (a) Low-energy spectrum for the effective two Kondo-impurity model describing a triangulene spin chain (TSC) on a superconductor (cf. Fig. 2). (b) Low-energy spectrum of the mesoscopic device that “quantum simulates” the TSC on a Superconductor (cf. Fig. 3) (c) Blow up of the avoided crossing of spin-singlet states for the molecular chain. The minimum gap between the states is controlled by the scattering potentials  $V_1$  and  $V_2$  that break particle-hole symmetry (d) Blow up of the avoided crossing for the device. The minimum gap is controlled by the junction tunneling amplitude.

since it depends on the inter-impurity distance and orientation relative to the substrate. Instead, in the VBS phase, the sign (ferromagnetic (FM) or antiferromagnetic (AFM)) and strength of the effective Heisenberg exchange interaction between the edge states are tunable by controlling the chain length. [5, 15]. Moreover, since the exchange between the inner triangulenes ( $\sim 18$  meV [15]) is stronger than their effective Kondo exchange with the substrate, the coupling of the inner units to the substrate can be neglected [15]. Thus, we can model the TSC as a two-Kondo-impurity system with the impurities representing the spin- $\frac{1}{2}$  edge states. Furthermore, due to the van der Waals interaction between the molecule and an STM tip, it is possible to tune the Kondo exchange of the terminal triangulene units [18, 36–38]. Using these ‘tools’, we show that it is possible to tune the system into a regime in which an avoided crossing of two lowest-lying spin-singlet states occurs. Alternatively, by studying shorter (longer) TSCs, where the Heisenberg (Kondo) exchange dominates, it is possible to observe the system on either side of the avoided level-crossing, provided the edge states are sufficiently strongly coupled to the substrate [39].

As pointed above, using spin-singlets suppresses decoherence due to Overhauser fields [30–34]. Additionally, the superconducting nature of the platform provides further protection through the energy gap, enhancing the overall robustness and quantum coherence of the qubit. However, currently, the TSCs can only be probed using

STM, which may not be practical for the operation of the qubit. Nevertheless, we show below that the low-lying spectrum of the TSC-superconductor system (see Fig. 2(a)) can be “quantum simulated” in a triple quantum dot system coupled to a superconducting junction (see Fig. 3). In this device, the operation and readout of the qubit are feasible using current state-of-the-art electronics [40, 41].

**Model:** The Hamiltonian of the systems studied below can be generally written as

$$\begin{aligned}
 H &= H_0 + \sum_{\nu} J_{\nu} \mathbf{S}_{\nu} \cdot \mathbf{s}_{\nu} + J_{12} \mathbf{S}_1 \cdot \mathbf{S}_2 \\
 &+ V_{\nu} \sum_{\sigma} \int d\epsilon \rho(\epsilon) a_{\epsilon\sigma\nu}^{\dagger} a_{\epsilon\sigma\nu}, \\
 H_0 &= \sum_{\nu, \nu'} \int d\epsilon \rho(\epsilon) \left[ \sum_{\sigma} \epsilon S_{\nu\nu'}(\epsilon) a_{\epsilon\sigma\nu}^{\dagger} a_{\epsilon\sigma\nu'} \right. \\
 &\left. + \Delta \delta_{\nu\nu'} \left( a_{\epsilon\uparrow\nu}^{\dagger} a_{\epsilon\downarrow\nu'}^{\dagger} + \text{H.c.} \right) \right], \quad (1)
 \end{aligned}$$

where  $J_{\nu}$  and  $V_{\nu}$  are, respectively, the Kondo couplings and scattering potentials of the impurity at  $\mathbf{r} = \mathbf{r}_{\nu}$  ( $\nu = 1, 2$ );  $J_{12}$  is the (Heisenberg) exchange between the two impurities (edge states);  $\mathbf{S}_{\nu}$  is the impurity spin operator and  $\mathbf{s}_{\nu}$  the spin of the itinerant electrons at  $\mathbf{r} = \mathbf{r}_{\nu}$ . In addition,  $\rho(\epsilon) = \rho_0$  is the density of states in the normal state, which is assumed to be a constant  $\rho_0 = 1/(2D)$  ( $D$  is the bandwidth). For a TSC on a superconductor, the overlap matrix  $S_{\nu\nu'}(\epsilon)$  describes the quantum amplitude for an electron to propagate from  $\mathbf{r}_{\nu}$  to  $\mathbf{r}_{\nu'}$ ; hence  $S_{\nu\nu}(\epsilon) = 1$ . The detailed form of  $S_{12}(\epsilon)$  is not important. For instance, following Ref. [35], it can be obtained assuming that the single-particle states of the host are plane waves.

**Avoided crossing of spin-singlet states:** Panel (a) in Fig. 2 shows the low-lying spectrum obtained using NRG for AFM Heisenberg coupling  $J_{12} = \Delta$  as a function of one of the Kondo couplings,  $J_1$ . Notice the two lowest-lying (spin-singlet) states,  $S$  and  $S'$ , undergo an avoided level crossing for  $J_1 \simeq J_{\text{cr}}$  ( $J_{\text{cr}}/\Delta \simeq 21.26$ ) (see also panel (b)). This is a consequence of the breaking of particle-hole and the  $1 \leftrightarrow 2$  reflection symmetries, as anticipated in Ref. [35]. This work studied an RKKY-coupled ‘Shiba molecule’ with  $J_1 = J_2$  and did not report explicit numerical results for the avoided crossing in the case where  $J_1 \neq J_2$  and  $V_{\nu=1,2} \neq 0$ . Besides the spin-singlets, spin-doublets,  $D$  and  $D'$ , and a spin triplet,  $T$ , are found at higher excitation energies but still below the superconducting gap  $\Delta$ . Therefore, they should be observable in the subgap scanning-tunneling spectra.

Interestingly, the low-lying spectrum can be reproduced using a zero-bandwidth approximation [42] (ZBA, see also supplementary information), which *effectively* captures the breaking of the particle-hole symmetry. In the ZBA, the superconductor Hamiltonian ( $H_0$  in Eq. 1)

state	$(S, P)$	figure
Impurity singlet ( $S_0$ )	$(0, +1)$	
Kondo singlet ( $S_2$ )	$(0, +1)$	
Doublets ( $D_1, D_2$ )	$(\frac{1}{2}, -1)$	
Triplet ( $T$ )	$(1, +1)$	

TABLE I. Lowest-energy states in the zero-bandwidth approximation;  $S$  and  $P = (-1)^{N_F}$  are the spin and fermion parity quantum numbers, respectively ( $N_F$  is the total fermion number in the superconductor). Red and blue solid circles represent spin-singlet and spin-triplet states, respectively. Blue (orange) dots represent the Kondo-impurity (superconductor) sites.

is replaced by two fermion sites with a pairing potential:  $\Delta \sum_{\nu} c_{\nu\uparrow}^{\dagger} c_{\nu\downarrow} + \text{H.c.}$  The overlap  $\propto S_{\mu\nu}$  of the channel orbitals is described by a hopping term,  $H_{12} = -t_{12} \sum_{\sigma} c_{1\sigma}^{\dagger} c_{2\sigma} + \text{H.c.}$  [43]. For  $t_{12} = 0$ , the lowest-lying states are two (valence-bond) spin-singlets  $S_0$  and  $S_2$  (see table I) that cross for  $J_1 = J_{1cr}$  (see Fig. 1(b) and 1(d) in SI). However, for  $t_{12} > 0$ , an avoided crossing occurs for two spin-singlet states,  $S$  and  $S'$ , which are linear combinations of  $S_0$  and  $S_2$ . Similar considerations apply to the spin-doublets  $D$  and  $D'$  in terms of the doublets  $D_1$  and  $D_2$  shown in table I. For  $t_{12} = 0$ , the global particle-hole symmetry (PHS) is unbroken. The latter is defined as the transformation where  $c_{\nu\sigma} \rightarrow c_{\nu,-\sigma}^{\dagger}$  and therefore  $H_{12} \rightarrow -H_{12}$ . Thus, having  $t_{12} > 0$  breaks the global PHS, resulting in an avoided crossing [44]. Nevertheless, it is important to stress that, in real systems, the global PHS is not broken by the term  $\propto S_{12}$  in Eq. (1), but by the scattering potentials  $V_{\nu=1,2}$ . In other words, for  $V_{\nu=1,2} = 0$  and  $S_{12} \neq 0$ , a level crossing exists, as e.g. found in Ref. [35] for  $J_1 = J_2$ . Therefore, the ZBA [43] must be regarded as an effective description and careful comparison to NRG must be done.

To summarize, in the parameter regime shown in Figs. 2(a) and (c) an isolated manifold two lowest-lying states undergoing an avoided realizes a spin-singlet qubit in the TSC-superconductor system. The qubit could be mechanically operated by tuning the Kondo coupling at one end of the TSC using the STM [18, 36–38]. However, in practice, the characteristic frequencies at which the tip position can be modulated in a typical STM are several orders of magnitude smaller than the smallest gap between the states  $S'$  and  $S$  ( $\approx \Delta/100 \approx 0.01$  meV  $\approx 1$  GHz). Thus, generating quantum coherent superpositions of  $S$  and  $S'$  by mechanical driving may be rather challenging, not to mention performing readout measurements of the qubit [45]. Instead, below we propose a qubit realization in a mesoscopic device in which the system parameters can be electrically controlled.

**Mesoscopic device emulating the TSC-superconductor system:** Since the ZBA is capable of reproducing the low-lying spectrum of the TSC-

superconductor system using a tunneling term (see Fig. 1(d) from the SI and Fig. 2(a)), we use superconducting wires in a tunneling junction. Moreover, the edge states of the TSC can be replaced by a triple quantum dot [40, 41]. The resulting device (see Fig. 3) is described by Eq. (1) with  $S_{12} = -t_{12}/\epsilon$  and  $S_{\nu\nu} = 1$ . The triple dot is a minimal setup to engineer by super-exchange the AFM coupling  $\propto J_{12} > 0$  in Eq. (1). In such systems,  $J_{12}$  ranges from 0.1 to 0.01 meV (see e.g. [40, 41, 46, 47]). Roughly speaking, the charging energy of the central dot suppresses single-particle tunneling between outer quantum dots. This results in the low-lying level structure shown in Figs. 2(b,d), where the two spin-singlets are the lowest lying states, well separated from the spin-doublet and triplet states. Since the doublets have opposite fermion parity (cf. table I), this level arrangement makes our qubit proposal a bit more robust against quasi-particle poisoning than earlier proposals [48] [49]. NRG finds an avoided crossing between the two lowest-lying states of the device that are spin singlets. Their minimum separation is controlled by  $t_{12}$  rather than  $V_{1,2}$ . In the SI, we show that accounting for charge fluctuations within the Anderson model does not spoil the structure of the spectrum and the avoided crossing.

**Two-level model of the qubit:** Next we introduce and test an effective two-level model that describes the qubit dynamics as realized in the mesoscopic device discussed above (see Fig. 3). In the parameter regime shown in Figs. 2(c,d) with fixed  $J_2, \Delta, V_1, V_2$  and  $J_{12}$ , the following effective two-level Hamiltonian obtained can be

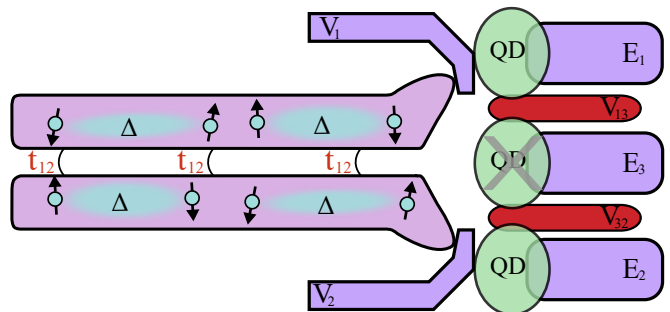


FIG. 3. Sketch of the mesoscopic device that emulates the TSC-superconductor system using a triple quantum dot system with the outer dots coupled to a junction of two superconducting wires. Seven gates,  $V_1, V_2, E_1, E_2, E_3, V_{13}$  and  $V_{32}$  define the dots and control the system parameters: The Kondo couplings,  $J_1$  and  $J_2$ , and the (AFM) super-exchange coupling  $J_{12}$ . The tunneling amplitude  $t_{12}$ , which can also be gate controlled, determines the size of the minimum gap at the avoided crossing of the two lowest-energy spin-singlets.

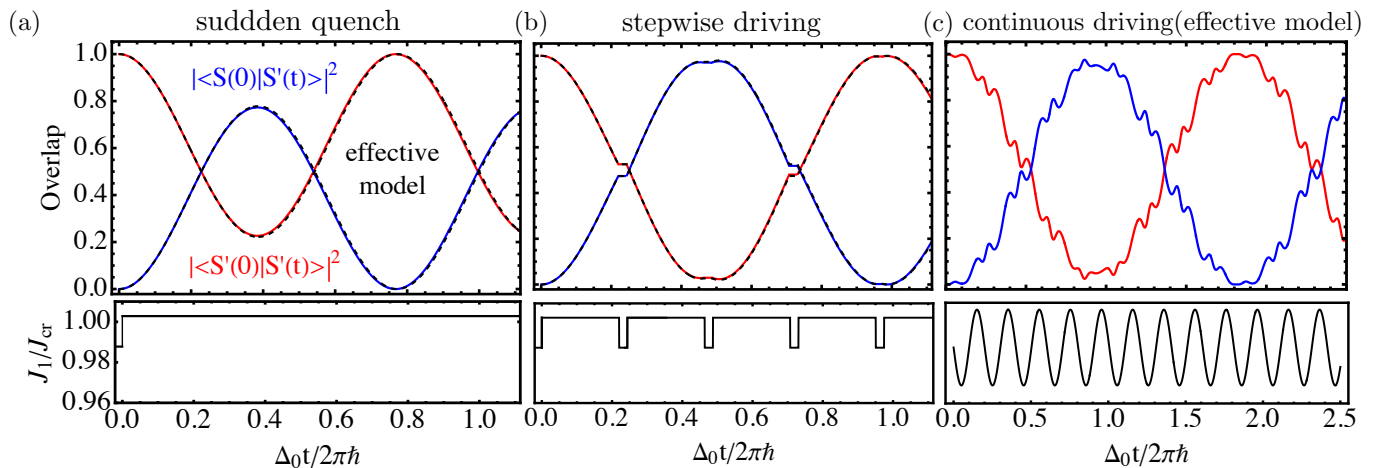


FIG. 4. Panels (a) and (b): Blue and Red lines are the overlaps between the time-evolved qubit state and the two initial singlet states computed using time-dependent NRG. The black dashed lines are the overlap derived from the effective two-level model in Eq. (2). The figures below are the corresponding quench profiles. (c) Overlap for a continuous driving calculated from the two-level effective model from Eq. (2).

introduced:

$$H_{\text{eff}} = [\epsilon_0 + \alpha(J_1(t) - J_0)] |S_2\rangle\langle S_2| + \frac{\Delta_0}{2} (|S_0\rangle\langle S_2| + |S_2\rangle\langle S_0|). \quad (2)$$

The basis of spin-singlet states  $\{|S_0\rangle, |S_2\rangle\}$  is defined for zero tunneling amplitude at the junction, i.e.  $t_{12} = 0$ , for which there is no avoided crossing. The parameter  $J_1(t)$  is the exchange coupling tuned by the gate  $V_1$  (see Fig. 3) that controls the tunneling ( $t_1$ ) between the upper quantum dot and closest superconducting wire of the junction ( $J_1 \propto t_1^2$  [17]);  $\epsilon_0 = E_{S_2} - E_{S_0}$  is the energy difference between the singlets for  $t_{12} = 0$ ;  $J_1(t=0) = J_0$  is the Kondo exchange of a reference (initial) state. We assume a linear dispersion of  $\epsilon_0$  for  $J_1 \simeq J_0$  and define  $\alpha = \frac{\partial \epsilon_0(J_1)}{\partial J_1}|_{J_1=J_0}$  in terms of the energy of  $|S_2\rangle$  at  $t_{12} = 0$  to take account for it. The off-diagonal term  $\Delta_0$  describes the coupling between the spin-singlet states induced by a finite  $t_{12}$ . All the parameters can be determined using NRG.

The validity of the effective model (2) is tested by comparing it to time-dependent NRG simulations of various scenarios. First, we consider a quantum quench where  $J_1(t)$  suddenly changes. The results shown in Fig. 4(a) assume the system is prepared in the ground state  $|S'\rangle$  with  $J_1/J_{cr} = 0.988$  and the Kondo coupling  $J_1$  is suddenly quenched to  $J_1/J_{cr} = 1.003$ . The overlap of the time-evolved state with the two initial spin-singlet states is thus computed both using the effective model (2) and time-dependent NRG for the full model described by Eq. (1). The effective model agrees well with the time-dependent NRG results. It is worth noticing that a sudden quench of  $J_1(t)$  conserves the total spin and, therefore, only states with the same spin as the initial state

(i.e., spin-singlets) can be excited during the time evolution. As the lowest-lying spin-singlets are well separated from other continuum states with zero total spin, the quench causes minimal admixture, and the dynamics are well reproduced by the effective two-level model from Eq. (2).

We have also considered more complex types of quenches. In Fig. 4(b), a step-wise drive where  $J_1(t)/J_{cr}$  oscillates between 0.988 and 1.003 with period  $T = 40.98 \times 2\pi\hbar/\Delta$ . The results from Eq. (2) accurately track the time-dependent NRG results.

**Driving and Readout:** In the following, we use the two-level model, Eq. (2), to show that Rabi oscillations between qubit states can be induced by a simple periodic modulation of one of the Kondo couplings where  $J_1(t) = J_1(0) + \delta J \sin(\omega t)$  with a fixed  $J_2$ . The corresponding oscillations is shown in Fig. 4(c), where  $J_1(t)/J_{cr}$  oscillates between  $0.988 \pm 0.0188$  with period  $T = 2\pi\hbar/\epsilon_0 = 33.87 \times 2\pi\hbar/\Delta$ . To avoid admixture with high energy states, the driving frequency must be much smaller than the superconducting gap:  $\omega = \epsilon_0 \ll \Delta/2\pi\hbar$ . The initial state is the ground state for  $J_1/\Delta = 21$  ( $J_1/J_{cr} = 0.988$ ). This driving protocol can be implemented in the setup of Fig. 3 using the gate electrodes connected to the quantum dots ( $V_1$  and  $V_2$  in Fig. 3), which govern the tunneling into/from the outer quantum dots, effectively modulating the Kondo exchange  $J_{1,2}$ . An oscillating electric field applied to the gate electrode could serve as the driving force. Notably, in this setup,  $J_1$  and  $J_2$  can be independently controlled, though this is not strictly necessary for qubit operation, as modulation of both couplings simultaneously is also viable. Readout can be achieved by measuring the absorption spectrum of an applied AC field [50, 51]. Absorption is maximized at the specific transition frequency, enabling precise char-

acterization of the qubit state. Similar to Ref. [52], the device in Fig. 3 can also be integrated into a cavity, allowing the readout of the qubit by coupling the cavity modes.

In conclusion, we have theoretically proposed a novel qubit platform that can be realized using a TSC grown on a superconducting substrate. However, to operate and read out the qubit, we have also introduced a mesoscopic device that quantum simulates the TSC-superconductor system. We have identified a parameter regime where the qubit has two lowest-lying spin-singlet states, which make the qubit immune to random magnetic fields. Although quasi-particle poisoning [53–56] can still be a source of decoherence, as it would give rise to a non-zero population of the states  $D_1$  and  $D_2$  in the QD. The already known schemes to avoid this perturbation can be implemented [54, 56, 57]. In connection to this, it is worth noting that, as the doublets lie above the spin-singlets, additional protection against quasi-particle poisoning is provided. Moreover, the simple readout mechanism outlined in the previous paragraph has successfully been used in state-of-the-art transmon-like qubits [50, 51].

We acknowledge useful discussions with F. S. Bergeret and J. I. Pascual. This work has been supported supported by the Agencia Estatal de Investigación (AEI) of the Ministerio de Ciencia, Innovación, y Universidades (Spain) through AEI/10.13039/501100011033 Grants No. PID2020-120614GB-I00 (ENACT) and No. PID2023-148225NB-C32 (SUNRISE). J. O. acknowledges the scholarship PRE\_2021\_1\_0350 from the Basque Government.

- 
- [1] T. Giamarchi, *Quantum Physics in One Dimension* (Oxford University Press, 2003).
- [2] F. D. M. Haldane, *Phys. Rev. Lett.* **50**, 1153 (1983).
- [3] F. Haldane, *Physics Letters A* **93**, 464 (1983).
- [4] I. Affleck, T. Kennedy, E. H. Lieb, and H. Tasaki, *Phys. Rev. Lett.* **59**, 799 (1987).
- [5] M. Hagiwara, K. Katsumata, I. Affleck, B. I. Halperin, and J. P. Renard, *Phys. Rev. Lett.* **65**, 3181 (1990).
- [6] A. Y. Kitaev, *Physics-Uspeski* **44**, 131 (2001).
- [7] F. Pollmann, E. Berg, A. M. Turner, and M. Oshikawa, *Phys. Rev. B* **85**, 075125 (2012).
- [8] S. Nadj-Perge, I. K. Drozdov, B. A. Bernevig, and A. Yazdani, *Phys. Rev. B* **88**, 020407 (2013).
- [9] S. Nadj-Perge, I. Drozdov, J. Li, H. Chen, S. Jeon, J. Seo, A. MacDonald, B. Bernevig, and A. Yazdani, *Science* **346**, 602 (2014), publisher Copyright: Copyright 2014 by the American Association for the Advancement of Science; all rights reserved.
- [10] L. Grill, M. Dyer, L. Lafferentz, M. Persson, M. V. Peters, and S. Hecht, *Nature Nanotech* **2**, 687 (2007).
- [11] A. Gourdon, *Angewandte Chemie* **47**, 6950 (2008).
- [12] N. Pavliek, A. Mistry, Z. Majzik, N. Moll, G. Meyer, D. J. Fox, and L. Gross, *Nature Nanotech* **12**, 308 (2017).
- [13] S. Mishra, D. Beyer, K. Eimre, J. Liu, R. Berger, O. Gröning, C. A. Pignedoli, K. Müllen, R. Fasel, X. Feng, and P. Ruffieux, *Journal of the American Chemical Society* **141**, 10621 (2019).
- [14] M. Vilas-Varela, F. Romero-Lara, A. Vegliante, J. P. Calupitan, A. Martínez, L. Meyer, U. Uriarte-Amiano, N. Friedrich, D. Wang, F. Schulz, *et al.*, *Angewandte Chemie* **135**, e202307884 (2023).
- [15] S. Mishra, G. Catarina, F. Wu, R. Ortiz, D. Jacob, K. Eimre, J. Ma, C. A. Pignedoli, X. Feng, P. Ruffieux, J. Fernandez-Rossier, and R. Fasel, *Nature* **598**, 287 (2021).
- [16] M. Hagiwara, K. Katsumata, I. Affleck, B. I. Halperin, and J. P. Renard, *Phys. Rev. Lett.* **65**, 3181 (1990).
- [17] A. Hewson, *The Kondo Problem to Heavy Fermions* (Cambridge University Press, Cambridge, 1993).
- [18] S. Trivini, J. Ortuzar, K. Vaxevani, J. Li, F. S. Bergeret, M. A. Cazalilla, and J. I. Pascual, *Phys. Rev. Lett.* **130**, 136004 (2023).
- [19] L. Schneider, C. von Bredow, H. Kim, K. T. Ton, T. Hnke, J. Wiebe, and R. Wiesendanger, “High-resolution spectroscopy of proximity superconductivity in finite-size quantized surface states,” (2024), [arXiv:2402.08895 \[cond-mat.supr-con\]](https://arxiv.org/abs/2402.08895).
- [20] L. Schneider, K. T. Ton, I. Ioannidis, J. Neuhaus-Steinmetz, T. Posske, R. Wiesendanger, and J. Wiebe, *Nature* **621**, 60 (2023).
- [21] K. Vaxevani, J. Li, S. Trivini, J. Ortuzar, D. Longo, D. Wang, and J. I. Pascual, *Nano Letters* **22**, 6075 (2022).
- [22] J.-C. Liu, R. Pawlak, X. Wang, H. Chen, P. D’Astolfo, C. Drechsel, P. Zhou, R. Hner, S. Decurtins, U. Aschauer, S.-X. Liu, W. Wulfhekel, and E. Meyer, *ACS Materials Lett.* **5**, 1083 (2023).
- [23] D. Loss and D. P. DiVincenzo, *Phys. Rev. A* **57**, 120 (1998).
- [24] C. Klocffel and D. Loss, *Annual Review of Condensed Matter Physics* **4**, 5181 (2013).
- [25] H. Drexler, D. Leonard, W. Hansen, J. P. Kotthaus, and P. M. Petroff, *Phys. Rev. Lett.* **73**, 2252 (1994).
- [26] S. Nadj-Perge, S. M. Frolov, E. P. A. M. Bakkers, and L. P. Kouwenhoven, *Nature* **468**, 1084 (2010).
- [27] J. W. G. van den Berg, S. Nadj-Perge, V. S. Pribiag, S. R. Plissard, E. P. A. M. Bakkers, S. M. Frolov, and L. P. Kouwenhoven, *Phys. Rev. Lett.* **110**, 066806 (2013).
- [28] M. Scheibner, M. Yakes, A. S. Bracker, I. V. Ponomarev, M. F. Doty, C. S. Hellberg, L. J. Whitman, T. L. Reinecke, and D. Gammon, *Nature Physics* **4**, 291 (2008).
- [29] A. Gaita-Ariño, F. Luis, S. Hill, and E. Coronado, *Nature Chemistry* **11**, 301 (2019).
- [30] N. E. Bonesteel, D. Stepanenko, and D. P. DiVincenzo, *Phys. Rev. Lett.* **87**, 207901 (2001).
- [31] G. Burkard and D. Loss, *Phys. Rev. Lett.* **88**, 047903 (2002).
- [32] W. A. Coish and D. Loss, *Phys. Rev. B* **70**, 195340 (2004).
- [33] J. Fischer, W. A. Coish, D. V. Bulaev, and D. Loss, *Phys. Rev. B* **78**, 155329 (2008).
- [34] J. Danon, A. Chatterjee, A. Gyenis, and F. Kuemmeth, *Applied Physics Letters* **119**, 260502 (2021), <https://pubs.aip.org/aip/apl/article-pdf/doi/10.1063/5.0073945/20031747/260502.1.5.0073945.pdf>.
- [35] N. Y. Yao, C. P. Moca, I. Weymann, J. D. Sau, M. D. Lukin, E. A. Demler, and G. Zaránd, *Phys. Rev. B* **90**, 241108 (2014).

- [36] K. J. Franke, G. Schulze, and J. I. Pascual, *Science* **332**, 940 (2011), <https://www.science.org/doi/pdf/10.1126/science.1202204>.
- [37] S. Karan, H. Huang, A. Ivanovic, C. Padurariu, B. Kubala, K. Kern, J. Ankerhold, and C. R. Ast, *Nat Commun* **15**, 459 (2024).
- [38] N. P. E. van Mullekom, B. Verlhac, W. M. J. van Weerdenburg, H. Osterhage, M. Steinbrecher, K. J. Franke, and A. A. Khajetoorians, *Science Advances* **10**, eadq0965 (2024), <https://www.science.org/doi/pdf/10.1126/sciadv.adq0965>.
- [39] This regime may be accessible in open ring TSCs in which the edge distance is small enough for the Kondo exchange of both edge states to be tuned using a single STM tip.
- [40] R. Sánchez, G. Granger, L. Gaudreau, A. Kam, M. Pioro-Ladrière, S. A. Studenikin, P. Zawadzki, A. S. Sachrajda, and G. Platero, *Phys. Rev. Lett.* **112**, 176803 (2014).
- [41] T. A. Baart, T. Fujita, C. Reichl, W. Wegscheider, and L. M. K. Vandersypen, *Nature Nanotech* **12**, 26 (2017).
- [42] F. von Oppen and K. J. Franke, *Phys. Rev. B* **103**, 205424 (2021).
- [43] H. Schmid, J. F. Steiner, K. J. Franke, and F. von Oppen, *Phys. Rev. B* **105**, 235406 (2022).
- [44] However, the ZBA does not require breaking reflection symmetry by having  $J_1 \neq J_2$  for the avoided crossing to occur, as it is not a complete description of the system; see SI.
- [45] An antenna emitting a microwave field could be used to control the qubit, similar to electron-spin resonance STM or atomic-force microscope (AFM) measurements in Refs. [58, 59]. However, new detection mechanisms would be required, as the singlet nature of the qubit prevents the readout via magnetoresistance changes [58]. Charge state variations could still be used [59].
- [46] K. Deng and E. Barnes, *Phys. Rev. B* **102**, 035427 (2020).
- [47] R. Sánchez, F. Gallego-Marcos, and G. Platero, *Phys. Rev. B* **89**, 161402 (2014).
- [48] G. O. Steffensen and A. L. Yeyati, “Ysr bond qubit in a double quantum dot with cqed operation,” (2024), [arXiv:2402.19261](https://arxiv.org/abs/2402.19261) [cond-mat.mes-hall].
- [49] Our NRG calculations of double quantum-dot system coupled by tunneling (rather than super-exchange) confirm [60] the results of Ref. [48], which were obtained in the infinite gap limit and yield a low-lying spectrum where the odd fermion-parity doublets lie between the even fermion-parity singlets [60].
- [50] C. Janvier, L. Tosi, L. Bretheau, . . . Girit, M. Stern, P. Bertet, P. Joyez, D. Vion, D. Esteve, M. F. Goffman, H. Pothier, and C. Urbina, *Science* **349**, 1199 (2015), <https://www.science.org/doi/pdf/10.1126/science.aab2179>.
- [51] M. Hays, V. Fatemi, D. Bouman, J. Cerrillo, S. Diamond, K. Serniak, T. Connolly, P. Krogstrup, J. Nygrd, A. L. Yeyati, A. Geresdi, and M. H. Devoret, *Science* **373**, 430 (2021), <https://www.science.org/doi/pdf/10.1126/science.abf0345>.
- [52] G. O. Steffensen and A. L. Yeyati, “YSR Bond Qubit in a Double Quantum Dot with cQED Operation,” .
- [53] J. Aumentado, G. Catelani, and K. Serniak, *Physics Today* **76**, 34 (2023).
- [54] J. M. Martinis, M. Ansmann, and J. Aumentado, *Phys. Rev. Lett.* **103**, 097002 (2009).
- [55] P. Joyez, P. Lafarge, A. Filipe, D. Esteve, and M. H. Devoret, *Phys. Rev. Lett.* **72**, 2458 (1994).
- [56] J. Aumentado, M. W. Keller, J. M. Martinis, and M. H. Devoret, *Phys. Rev. Lett.* **92**, 066802 (2004).
- [57] R.-P. Riwar, A. Hosseinkhani, L. D. Burkhardt, Y. Y. Gao, R. J. Schoelkopf, L. I. Glazman, and G. Catelani, *Phys. Rev. B* **94**, 104516 (2016).
- [58] S. Baumann, W. Paul, T. Choi, C. P. Lutz, A. Ardavan, and A. J. Heinrich, *Science* **350**, 417 (2015), <https://www.science.org/doi/pdf/10.1126/science.aac8703>.
- [59] L. Sellies, R. Spachtholz, S. Bleher, J. Eckrich, P. Scheuerer, and J. Repp, *Nature* **624**, 64 (2023).
- [60] C.-H. Huang, J. Ortuzar, and M. A. Cazalilla, ((2025)).

# Supplementary Material for "Superconducting Spin-Singlet QuBit in a Triangulene Spin Chain"

Chen-How Huang,<sup>1,2</sup> Jon Ortuzar,<sup>3</sup> and M. A. Cazalilla<sup>1,4</sup>

<sup>1</sup>*Donostia International Physics Center (DIPC),  
20018 Donostia-San Sebastián, Spain*

<sup>2</sup>*Departamento de Polmeros y Materiales Avanzados: Física,  
Química y Tecnología, Facultad de Ciencias Químicas,  
Universidad del País Vasco UPV/EHU,  
20018 Donostia-San Sebastián, Spain.*

<sup>3</sup>*CIC nanoGUNE-BRTA, 20018 Donostia-San Sebastián, Spain*

<sup>4</sup>*IKERBASQUE, Basque Foundation for Science,  
Plaza Euskadi 5 48009 Bilbao, Spain*

(Dated: April 1, 2025)

## CONTENTS

Zero-Bandwidth Approximation (ZBA)	2
Assessment of the Effect of Charge Fluctuations	3
Details of the NRG Calculations	4
Details of the Time-dependent NRG Calculations	6
Level crossing between the two sub-gap singlet states	8
References	9

## ZERO-BANDWIDTH APPROXIMATION (ZBA)

The ZBA [1–3] can be used to qualitatively describe the low-lying spectrum of the system. In the ZBA, the Hamiltonian reads:

$$H = H_0 + H_S + H_t \quad (1)$$

$$H_0 = \Delta \sum_{\alpha=1,2} \left[ c_{\alpha\uparrow}^\dagger c_{\alpha\downarrow}^\dagger + \text{H.c.} \right] \quad (2)$$

$$H_S = J_{12} \mathbf{S}_1 \cdot \mathbf{S}_2 + \sum_{\alpha=1,2} J_\alpha \mathbf{S}_\alpha \cdot c_{\alpha s}^\dagger \boldsymbol{\sigma} c_{\alpha s'} \quad (3)$$

$$H_t = -t_{12} \sum_s \left[ c_{1\sigma}^\dagger c_{2\sigma} + \text{H.c.} \right], \quad (4)$$

where,  $c_{\alpha s}^\dagger$  ( $c_{\alpha s}$ ) is the creation (annihilation) operator of an electron with spin  $s$  in the  $\alpha$  site,  $\Delta$  is the superconducting pairing energy,  $J_\alpha$  are the exchange coupling of the edge states with the substrate,  $J_{12}$  is the exchange interaction between the spins, and  $t_{12}$  is a hopping term between superconductors, which accounts for the extension of the YSR states [3].

The lowest-lying states described by the ZBA Hamiltonian for  $t_{12} = 0$  are listed in table 1 of the main text. The phase diagram, as a function of the exchange coupling between edge states and the substrate, is shown in Fig. 1(a). Notably, for a finite  $J_{12}$ , a transition between the two spin-singlet states takes place along the trajectory in parameter space indicated by the black dashed line. The evolution of the energy of the four lowest-energy states along this trajectory is shown in Fig. 1(b), where a (level-crossing) quantum phase transition occurs between the  $S_0$  and  $S_2$  states, while the doublet states remain well separated at higher energy. This can be regarded as a non-local quantum phase transition, since the actions on the exchange coupling of one impurity can generate a global transition where both impurities capture a quasi-particle from their respective superconducting baths.

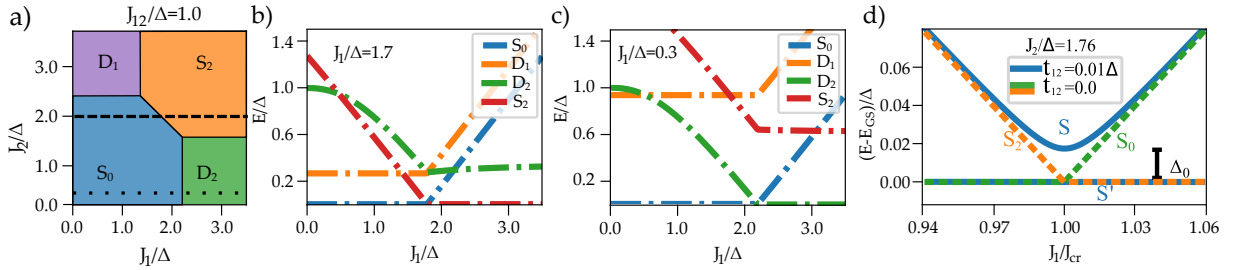


FIG. 1. **ZBA results.** (a) Phase diagram of the two impurity model for  $J_{12} = \Delta$  and  $t_{12} = 0$  as a function of the individual exchange couplings with the substrate,  $J_1$  and  $J_2$ . (b) and (c) Evolution of the energy of the four lowest-lying states along the dashed and dotted lines in panel (a), respectively. (d) Comparison between no hopping (dashed lines) and a small hopping term (solid line) in the vicinity of the  $S_0 \rightarrow S_2$  transition in panel (a).

Additionally, the parity-changing quantum phase transition [1, 4–6] is accessible along the dotted black line in Fig. 1(a). The corresponding spectrum evolution is shown in Fig. 1(c), highlighting the parity change of the ground state between the  $S_0$  and  $D_2$  states.



As introduced in the main text, the hopping term  $t_{12}$  breaks global particle-hole symmetry, mixing the two singlet states by generating a finite matrix element between  $S_0$  and  $S_2$ . Consequently, the new eigenstates, denoted as  $S$  and  $S'$ , emerge as linear combinations of  $S_0$  and  $S_2$ . This mixing results in an avoided crossing of the spin-singlet states, as shown in Fig. 1(d). This figure resembles the results obtained by NRG calculation (see Fig. 2 in the main text, demonstrating the ZBA can effectively describe the evolution of the low-energy spectrum of the system as a function of the the Kondo exchange of one of the impurities.

## ASSESSMENT OF THE EFFECT OF CHARGE FLUCTUATIONS

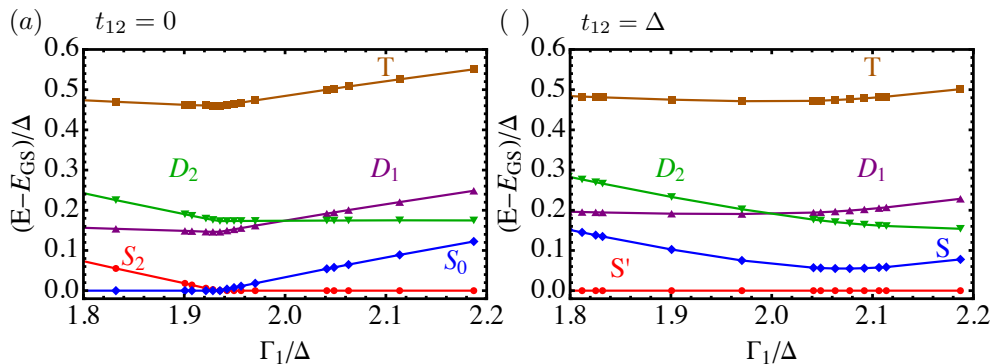


FIG. 2. NRG results for the effective model (cf. Eq. 5) of a triple quantum quantum dot device for  $U_1 = U_2 = 8\Delta$ ,  $\epsilon = -0.5U$ ,  $\Gamma_2 = 1.999\Delta$ ,  $J_{12} = \Delta$  and  $\Delta = D/400$  where  $D$  is the band cut-off.  $\Gamma_i = \pi t_i^2 \rho_0$  is the hopping rate. The inter bath hoppings are (a)  $t_{12} = 0$  (b)  $t_{12} = \Delta$ .

In the main text, we have used an effective Kondo Hamiltonian to describe the coupling of the triple quantum dot system to the superconductors in a junction. In this section, we use the more fundamental Anderson model in order to assess the effect of charge fluctuations in the outer dots of the triple-dot system. To this end, we study the following *minimal* model of two Anderson impurities coupled to each other by super-exchange and tunnel coupled to two superconductors in a junction:

$$H = J_{12} \mathbf{S}_1 \cdot \mathbf{S}_2 - t_{12} \left( c_{\mathbf{k}\sigma 1}^\dagger c_{\mathbf{k}\sigma 2} + \text{H.c.} \right) + \sum_{\alpha=1,2} H_\alpha \quad (5)$$

$$H_\alpha = U \left( n_{d;\uparrow\alpha} - \frac{1}{2} \right) \left( n_{d;\downarrow\alpha} - \frac{1}{2} \right) - t_\alpha \sum_{\mathbf{k}\sigma} \left( d_\alpha^\dagger c_{\mathbf{k}\sigma\alpha} + \text{H.c.} \right) \quad (6)$$

$$+ \sum_{\mathbf{k}} \left[ \sum_{\sigma} \epsilon_{\mathbf{k}} c_{\mathbf{k}\sigma\alpha}^\dagger c_{\mathbf{k}\sigma\alpha} + \Delta (c_{\mathbf{k}\uparrow\alpha} c_{\mathbf{k}\downarrow\alpha} + \text{H.c.}) \right].$$

Here  $d_{\sigma\alpha}$  ( $d_{\sigma\alpha}^\dagger$ ) is the annihilation (creation) operator for electrons in the dot and  $c_{\mathbf{k}\sigma\alpha}$  ( $c_{\mathbf{k}\sigma\alpha}^\dagger$ ) is the annihilation (creation) operator for electrons in the superconductor  $\alpha = 1, 2$  with s-wave pairing potential proportional to  $\Delta$ .  $U$  is the onsite coulomb interaction strength. We

use the symmetric Anderson model to describe the dots. The global particle-hole symmetry is broken by the junction tunneling term  $\propto t_{12}$ .

Carrying out the calculation of the low-energy spectrum using NRG, we still find a parameter regime accessible by tuning the tunneling into one of the dots where the two lowest energy states are spin-singlets and undergo an avoided crossing, see Fig. 2. Notice that, as shown in the figure, the avoided crossing is observed for finite  $t_{12}$  between the two superconductors.

## DETAILS OF THE NRG CALCULATIONS

In order to carry out the Numerical Renormalization Group (NRG) calculations of the low-energy spectrum, the Hamiltonian of the bath in Eq. (1) of the main text is discretized logarithmically using the adaptive scheme [7] with discretization parameter  $\Lambda = 4$  assuming a constant density of states  $\rho = 1/(2D)$ . This procedure yields the following Wilson-chain Hamiltonian for the superconducting host:

$$H = H_0 + \tilde{H}_{12}^X \quad (7)$$

$$H_0 = H_{\text{imp}} + \tilde{H}_1 + \tilde{H}_2, \quad (8)$$

$$H_{\text{imp}} = J_{12} \mathbf{S}_1 \cdot \mathbf{S}_2 + J_1 \mathbf{S}_1 \cdot \mathbf{s}_1 + J_2 \mathbf{S}_2 \cdot \mathbf{s}_2. \quad (9)$$

$$\begin{aligned} \tilde{H}_\alpha = & V_\alpha n_\alpha(0) - \sum_i t_i [f_{\alpha\sigma}(i) f_{\alpha\sigma}^\dagger(i+1) + f_{\alpha\sigma}(i+1) f_{\alpha\sigma}^\dagger(i)] \\ & + \Delta [f_{\alpha\uparrow}(i) f_{\alpha\downarrow}(i) + f_{\alpha\uparrow}^\dagger(i) f_{\alpha\downarrow}^\dagger(i)], \end{aligned} \quad (10)$$

where  $t_i \sim \Lambda^{-i/2}$  decays exponentially. We note the Hamiltonian,  $H_0$ , for  $V_\alpha \neq 0$  only preserves the SU(2) spin symmetry. On the contrary, if  $V_\alpha = 0$ , there is a hidden U(1) charge symmetry [8, 9],  $Q_{X;\alpha} = (Q_{+;\alpha} + Q_{-;\alpha})/2$ , where

$$Q_{+;\alpha} = \sum_i (-1)^i f_{\alpha\uparrow}^\dagger(i) f_{\alpha\downarrow}^\dagger(i), \quad (11)$$

$$Q_{-;\alpha} = Q_{+;\alpha}^\dagger. \quad (12)$$

This U(1) symmetry will be exploited for the device.

$\tilde{H}_{12}^X$  denotes the term in the Hamiltonian coupling the two superconducting baths (channels). For the TSC-superconductor system,

$$\tilde{H}_{12}^{\text{TSC}} = -t_i \mathcal{S}_{12} \sum_{i\sigma} [f_{1\sigma}(i) f_{2\sigma}^\dagger(i+1) + f_{2\sigma}(i) f_{1\sigma}^\dagger(i+1) + \text{H.c.}] \quad (13)$$

where  $\mathcal{S}_{12} = \mathcal{S}(\epsilon_F)$  is the quantum amplitude for the electrons at the Fermi level to propagate

from impurity 1 to impurity 2 [8]. However, for the device

$$\tilde{H}_{12}^{\text{QD}} = -t_{12} \sum_{i\sigma} \left[ f_{1\sigma}(i) f_{2\sigma}^\dagger(i) + f_{2\sigma}(i) f_{1\sigma}^\dagger(i) \right]. \quad (14)$$

For the calculation of the low-energy spectrum and the time evolution of the device, we set  $V_\alpha = 0$ . In this limit, we further simplify the Hamiltonian following the method described in [10] which is a rotation in the conserved  $Q_X = \sum_\alpha Q_{X;\alpha} (-1)^\alpha$ . We apply the following Bogoliubov transformation:

$$b_{\alpha\uparrow}^\dagger(i) = \frac{1}{\sqrt{2}} \left( f_{\alpha\uparrow}^\dagger(i) + f_{\alpha\downarrow}(i) \right), \quad (15)$$

$$b_{\alpha\downarrow}(i) = \frac{1}{\sqrt{2}} \left( f_{\alpha\uparrow}^\dagger(i) - f_{\alpha\downarrow}(i) \right), \quad (16)$$

followed by a particle-hole transformation for chain 1:

$$c_{1\uparrow}^\dagger(2i) = b_{1\uparrow}^\dagger(2i), \quad (17)$$

$$c_{1\downarrow}(2i) = b_{1\downarrow}(2i), \quad (18)$$

$$c_{1\uparrow}^\dagger(2i-1) = b_{1\downarrow}(2i-1), \quad (19)$$

$$c_{1\downarrow}(2i-1) = -b_{1\uparrow}^\dagger(2i-1). \quad (20)$$

And for chain 2:

$$c_{2\uparrow}^\dagger(2i-1) = b_{2\uparrow}^\dagger(2i-1), \quad (21)$$

$$c_{2\downarrow}(2i-1) = b_{2\downarrow}(2i-1), \quad (22)$$

$$c_{2\uparrow}^\dagger(2i) = b_{2\downarrow}(2i), \quad (23)$$

$$c_{2\downarrow}(2i) = -b_{2\uparrow}^\dagger(2i). \quad (24)$$

which yields the following Wilson-chain Hamiltonian:

$$H = H_{\text{imp}} + \tilde{H}'_1 + \tilde{H}'_2 + \tilde{H}'_{12}{}^{\text{QD}}, \quad (25)$$

$$\tilde{H}'_\alpha = \sum_i \left\{ t_i \sum_\sigma \left( c_{\alpha\sigma}(i) c_{\alpha\sigma}^\dagger(i+1) + h.c. \right) - \Delta (-1)^{i+\alpha} Q_{Z;\alpha}(i) \right\}. \quad (26)$$

and

$$\tilde{H}'_{12}{}^{QD} = -t_{12} \sum_{\sigma} \left[ c_{2\sigma}(i) c_{1\sigma}^{\dagger}(i) + c_{1\sigma}(i) c_{2\sigma}^{\dagger}(i) \right]. \quad (27)$$

The NRG for the model in Eq. (1) with constant overlap matrix  $\mathcal{S}_{12}$  (corresponding to the TSC-superconductor system) is performed using the conserved SU(2) spin,  $S$ . For the device, we used both the SU(2) spin and U(1) charge isospin quantum numbers ( $S, Q_Z$ ):

$$Q_Z = Q_{Z;1} + Q_{Z;2}, \quad (28)$$

$$Q_{Z;\alpha} = \sum_i Q_{Z;\alpha}(i) = \frac{1}{2} \sum_i [n_{\alpha\uparrow}(i) + n_{\alpha\downarrow}(i) - 1]. \quad (29)$$

$$S = \sum_{\alpha} \left[ S_{\alpha}^{\text{imp}} + \sum_i S_{\alpha}(i) \right]. \quad (30)$$

We keep at most 5,000 multiplets ( $\sim 15,000$  states) for the spectrum and evolution of the device. In the presence of gap, the NRG iteration should be truncated at iterations with energy scale  $\omega_N \ll \Delta$  [11]. We stop our NRG computation at iterations with energy scale  $\sim 10^{-9}\Delta$  and use a temperature  $T \ll \Delta$  as an effective zero-temperature limit.

## DETAILS OF THE TIME-DEPENDENT NRG CALCULATIONS

In this section, we provide the details of the time-dependent NRG calculation for the overlap after a multiple quench. For the quench profiles of the series of Hamiltonians  $H_0, H_1, \dots, H_n$  with periods  $t_0 = 0, t_1, \dots, t_n$  starting from initial states  $|l_0 e_0^N N\rangle$  and  $|l'_0 e_0^N N\rangle$  where  $|l_i e_i N\rangle$  denotes the state of Hamiltonian  $H_i$  at the last iteration  $N$  labeled by  $l_i$  and the environment index  $e_i$ . By the definition, within the Full-Density Matrix NRG (FDM-NRG) [12], all states are discarded at the last iteration. The overlap at time  $t = t_1 + t_2 + \dots + t_n$  reads

$$P_{l_0 l'_0}(t) = \langle l'_0 e_0^N N | e^{-iH_n t_n} \dots e^{-iH_1 t_1} | l_0 e_0^N N \rangle. \quad (31)$$

Next, we insert the complete basis[13, 14] for each NRG of Hamiltonian  $H_i$ :

$$1_i = \sum_{l_i e_i m_i} |l_i e_i m_i\rangle \langle l_i e_i m_i|, \quad (32)$$

$$= \sum_{l_i e_i m_i < m'_i} |l_i e_i m_i\rangle \langle l_i e_i m_i| + \sum_{s_i e_i} |s_i e_i m'_i\rangle \langle s_i e_i m'_i|. \quad (33)$$

where  $l_i$  are the labels for all the discarded states at iteration  $m_i$  and  $s_i$  labels both the discarded and kept states.  $e_i$  is the index for the environment basis. Both of the identities

will be used in the following derivation. Using the first equation, we get,

$$P_{l_0 l'_0} = \sum_{l_n, e_n, m_n} \cdots \sum_{l_2, e_2, m_2} \sum_{l_1, e_1, m_1} {}_0 \langle l'_0 e_0^N N | l_n e_n m_n \rangle \langle l_n e_n m_n | e^{-iH_n t_n} \cdots \\ |l_2 e_2 m_2 \rangle \langle l_2 e_2 m_2 | e^{-iH_2 t_2} | l_1 e_1 m_1 \rangle \langle l_1 e_1 m_1 | e^{-iH_1 t_1} | l_0 e_0^N N \rangle_0. \quad (34)$$

Using the NRG approximation  $\langle l_i e_i m_i | e^{-iH_i t_i} = \langle l_i e_i m_i | e^{-i\epsilon(l_i, m_i) t_i}$  where  $\epsilon(l_i, m_i)$  is the eigenvalue of the eigenstate  $\langle l_i e_i m_i |$  and the following identity for the multiple sums[15]:

$$\sum_{l_n, e_n, m_n} \cdots \sum_{l_2, e_2, m_2} \sum_{l_1, e_1, m_1} = \sum_{r_1, r_2, \dots, r_n}^{\neq K_1, K_2, \dots, K_n} \sum_{e_1, e_2, \dots, e_n} \sum_m \quad (35)$$

In the r.h.s,  $r_1, \dots, r_n$  can be either kept or discarded states, and they can not be all kept states in the summation. We have

$$P_{l_0 l'_0} = \sum_{r_1, r_2, \dots, r_n}^{\neq K_1, K_2, \dots, K_n} \sum_{e_1, e_2, \dots, e_n} \sum_m \langle l'_0 e_0^N N | r_n e_n m \rangle \langle r_n e_n m | r_{n-1} e_{n-1} m \rangle e^{-i\epsilon(r_n, m) t_n} \cdots, \\ \times |r_2 e_2 m \rangle e^{-i\epsilon(r_2, m) t_2} \langle r_2 e_2 m | r_1 e_1 m \rangle e^{-i\epsilon(r_1, m) t_1} \langle r_1 e_1 m | l_0 e_0^N N \rangle, \quad (36)$$

$$= \sum_{r_1, r_2, \dots, r_n}^{\neq K_1, K_2, \dots, K_n} \sum_{e_1, e_2, \dots, e_n} \sum_m \langle l'_0 e_0^N N | r_n e_n m \rangle S_{r_n, r_{n-1}}(m) \delta_{e_n, e_{n-1}} e^{-i\epsilon(r_n, m) t_n} \cdots \\ \times e^{-i\epsilon(r_2, m) t_2} S_{r_2, r_1}(m) \delta_{e_2, e_1} e^{-i\epsilon(r_1, m) t_1} \langle r_1 e_1 m | l_0 e_0^N N \rangle, \quad (37)$$

$$= \sum_{r_1, r_2, \dots, r_n}^{\neq K_1, K_2, \dots, K_n} \sum_e \sum_m \langle r_1 e m | l_0 e_0^N N \rangle \langle l'_0 e_0^N N | r_n e m \rangle \times \\ S_{r_n, r_{n-1}}(m) e^{-i\epsilon(r_n, m) t_n} \cdots e^{-i\epsilon(r_2, m) t_2} S_{r_2, r_1}(m) e^{-i\epsilon(r_1, m) t_1}, \quad (38)$$

where  $S_{r_n r_{n-1}}(m) \delta_{e_n, e_{n-1}} = \langle r_n e_n m | r_{n-1} e_{n-1} m \rangle$  is the overlap matrix element between NRG eigenstates of different Hamiltonians[14]. Next, we calculate the following matrix element

by inserting the second identity in Eq. (33)

$$\sum_e \langle r_1 em | l_0 e_0^N N \rangle \langle l'_0 e_0^N N | r_n em \rangle, \quad (39)$$

$$= \sum_e \langle r_1 em | \left[ \sum_{l_0 e_0 m_0 < m} |l_0 e_0 m_0\rangle \langle l_0 e_0 m_0| + \sum_{s_0 e_0} |s_0 e_0 m\rangle \langle s_0 e_0 m| \right] |l_0 e_0^N N\rangle$$

$$\times \langle l'_0 e_0^N N | \left[ \sum_{l_0 e_0 m_0 < m} |l_0 e_0 m_0\rangle \langle l_0 e_0 m_0| + \sum_{s_0 e_0} |s_0 e_0 m\rangle \langle s_0 e_0 m| \right] |r_n em\rangle \quad (40)$$

$$= \sum_e \sum_{s_0 e_0} \sum_{s'_0 e'_0} \langle r_1 em | s_0 e_0 m \rangle \langle s_0 e_0 m | l_0 e_0^N N \rangle \langle l'_0 e_0^N N | s'_0 e'_0 m \rangle \langle s'_0 e'_0 m | r_n em \rangle \quad (41)$$

$$= \sum_e \sum_{s_0 e_0} \sum_{s'_0 e'_0} S_{r_1 s_0}(m) \delta_{e, e_0} \langle s_0 e_0 m | l_0 e_0^N N \rangle \langle l'_0 e_0^N N | s'_0 e'_0 m \rangle S_{s'_0 r_n}(m) \delta_{e'_0, e} \quad (42)$$

$$= \sum_{s_0 s'_0} S_{r_1 s_0}(m) \left[ \sum_e \left[ A_{l_0 e_0^N \rightarrow s_0 e}^{N \rightarrow m} \right]^\dagger O_{l_0 l'_0}(N) A_{l'_0 e_0^N \rightarrow s'_0 e}^{N \rightarrow m} \right] S_{s'_0 r_n}(m) \quad (43)$$

$$= \sum_{s_0 s'_0} S_{r_1 s_0}(m) O_{l_0 l'_0 \rightarrow s_0 s'_0}^{red}(m) S_{s'_0 r_n}(m) \quad (44)$$

where  $O_{l_0 l'_0}(N) = |l_0 e_0^N N\rangle \langle l'_0 e_0^N N|$  is the matrix element at the last iteration of NRG on  $H_0$  and  $O_{l_0 l'_0 \rightarrow s_0 s'_0}^{red}(m)$  is the reduced matrix element which is calculated by the tensor product of the unitary transformations  $A_{l_e \rightarrow l'_e}^{n \rightarrow n-1}$  calculated from each NRG iteration of  $H_0$  and tracing out the environment basis[12]. Combining Eq. (39) and (44). The overlap is

$$P_{l_0 l'_0} = \sum_{r_1, r_2, \dots, r_n}^{\neq K_1, K_2, \dots, K_n} \sum_m \sum_{s_0 s'_0} e^{-i\epsilon(r_n, m)t_n} S_{r_n, r_{n-1}}(m) \times \dots \quad (45)$$

$$\times e^{-i\epsilon(r_1, m)t_1} S_{r_1 s_0}(m) O_{l_0 l'_0 \rightarrow s_0 s'_0}^{red}(m) S_{s'_0 r_n}(m).$$

To compute this, we first compute all the NRG eigenvectors and eigenvalues for the Hamiltonians,  $H_0, \dots, H_n$ . Then use the eigenvectors to compute all the necessary overlap matrix element,  $S_{ij}$  and the reduced matrix elements,  $O^{red}$ . Finally insert everything into Eq. (45).

## LEVEL CROSSING BETWEEN THE TWO SUB-GAP SINGLET STATES

In this section, we discuss the low-energy energy spectrum obtained when setting  $\mathcal{S}_{12} = 0$  and  $V_{1,2} = 0$  in Eq. (1) of the main text. The Wilson chain Hamiltonian reads,  $H = H_{\text{imp}} + \tilde{H}_1 + \tilde{H}_2$  which are defined in Eq. (7).

In this case, as shown in panel (a) of Fig. 3, a phase boundary between two phases whose ground states are adiabatically connected to  $S_0$  and  $S_2$  in table 1 exist. These two spin-

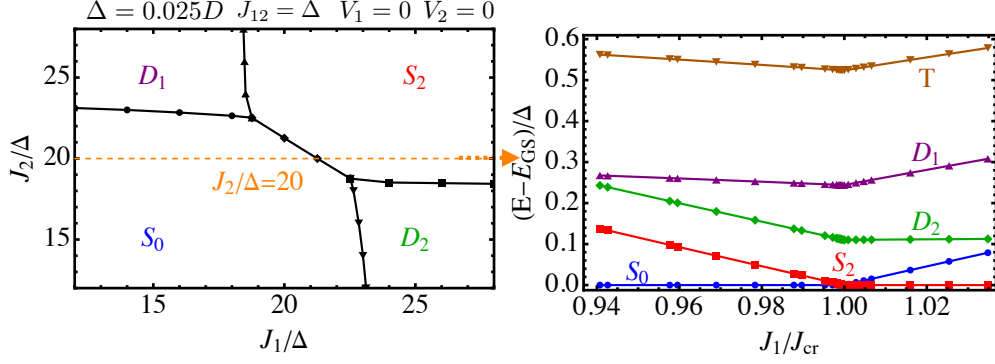


FIG. 3. NRG results for Eq. (1) of the main text with  $S_{12} = 0$ , i.e. two independent superconducting baths. (a) the phase diagram for  $J_{12} = \Delta, V_1 = V_2 = 0$ . (b) Sub-gap energy levels related to the ground state along  $J_2/\Delta = 20$ .

singlet states become degenerate at this boundary as shown in panel (b) of the same figure. The latter displays the evolution of the low-energy spectrum along the path shown in panel (a) as a dashed line, along which  $J_2/\Delta = 20$  while  $J_1$  is varied. This level crossing is the nonlocal quantum phase transition, which was discussed above using the ZBA.

- 
- [1] F. von Oppen and K. J. Franke, *Phys. Rev. B* **103**, 205424 (2021).
- [2] J. Ortuzar, J. I. Pascual, F. S. Bergeret, and M. A. Cazalilla, *Phys. Rev. B* **108**, 024511 (2023).
- [3] H. Schmid, J. F. Steiner, K. J. Franke, and F. von Oppen, *Phys. Rev. B* **105**, 235406 (2022).
- [4] L. Yu, *Acta Physica Sinica* **21**, 75 (1965).
- [5] H. Shiba, *Prog. Theor. Phys.* **40**, 435 (1968).
- [6] A. I. Rusinov, *Sov. J. Exp. Theor. Phys.* **29**, 1101 (1969).
- [7] R. Žitko, *Computer Physics Communications* **180**, 1271 (2009).
- [8] N. Y. Yao, C. P. Moca, I. Weymann, J. D. Sau, M. D. Lukin, E. A. Demler, and G. Zaránd, *Phys. Rev. B* **90**, 241108 (2014).
- [9] A. I. Tóth, C. P. Moca, O. Legeza, and G. Zaránd, *Phys. Rev. B* **78**, 245109 (2008).
- [10] K. Satori, H. Shiba, O. Sakai, and Y. Shimizu, *Journal of the Physical Society of Japan* **61**, 3239 (1992), <https://doi.org/10.1143/JPSJ.61.3239>.
- [11] T. Hecht, A. Weichselbaum, J. von Delft, and R. Bulla, *Journal of Physics: Condensed Matter* **20**, 275213 (2008).
- [12] A. Weichselbaum and J. von Delft, *Phys. Rev. Lett.* **99**, 076402 (2007).

- [13] F. B. Anders and A. Schiller, [Phys. Rev. Lett. \*\*95\*\*, 196801 \(2005\)](#).
- [14] F. B. Anders and A. Schiller, [Phys. Rev. B \*\*74\*\*, 245113 \(2006\)](#).
- [15] I. Weymann, J. von Delft, and A. Weichselbaum, [Phys. Rev. B \*\*92\*\*, 155435 \(2015\)](#).